A C–H Activation-Based Enantioselective Synthesis of Lower Carbo[*n*]helicenes (*n* = 4-6)

Shu-Min Guo,[1] Soohee Huh,[1] Max Coehlo,[2] Li Shen,[1] Grégory Pieters,[2] and Olivier Baudoin[1]*

[1]University of Basel, Department of Chemistry, St. Johanns-Ring 19, CH-4056 Basel, Switzerland.

[2]Université Paris-Saclay, CEA, INRAE, Département Médicaments et Technologies pour la Santé (DMTS), SCBM, F-91191, Gif-sur-Yvette, France.

*e-mail: olivier.baudoin@unibas.ch

Abstract: The unique three-dimensional structure of carbohelicenes have fascinated generations of molecular chemists and has been exploited through a wide range of applications. In particular, their strong circularly polarized luminescence (CPL) has raised much attention in recent years due to promising applications in the design of new optical materials. Whereas a number of important precedents report enantioselective syntheses of fused carbo- and heterohelicenes, a direct catalytic enantioselective method allowing the synthesis of lower, nonfused carbo[*n*]helicenes (*n* = 4-6) is still lacking. We report that Pd-catalysed enantioselective C–H arylation in the presence of a unique bifunctional phosphine-carboxylate ligand provides a simple and general access to these simple carbo[*n*]helicenes. Computational mechanistic studies indicate that both the C–H activation and reductive elimination steps contribute to the overall enantioselectivity. In addition, the observed enantio-induction seems to arise from a combination of noncovalent interactions and steric repulsion between the substrate and ligand during the two key reductive elimination steps. Moreover, the current method allows a comparative study of the CPL properties of lower carbo[*n*]helicenes, which led to the discovery that carbo[*4*]helicenes actually display CPL responses comparable to the higher carbo[*6*]helicene congeners.

Introduction

Carbohelicenes are polycyclic aromatic compounds composed of consecutive *ortho*-fused benzene rings, which adopt a nonplanar, helical topology.[1] The great steric hindrance between the two terminal rings may result in a pair of configurationally stable (*M*) and (*P*) enantiomers and the presence of a stereogenic helix axis (Fig. 1a). This particular topology has been widely exploited[2] in diverse fields ranging from asymmetric catalysis,[3] to optoelectronic devices,[4] stereochemical molecular recognition[5] and photodynamic therapy.[6] In particular, the highly distorted conjugated π-system of carbohelicenes and their heteroatomic analogues[7] termed heterohelicenes provide them with strong chiroptical properties, including circularly polarized luminescence (CPL),[8] which have raised much interest in recent years due to promising applications in the design of new optical materials. The unique topology and properties of helicenes have fascinated synthetic chemists for decades.[9,10] Despite major achievements in enantioselective synthesis, the resolution of racemic mixtures is still the dominant method to obtain optically pure helicenes and study their chiroptical properties.[11] Enantioselective catalysis, which is ultimately the most desirable method to access a given nonracemic helicene, has markedly developed in recent years and important advances have been reported. In particular, both organocatalysis[12,13] and transition-metal catalysis,[14–17] proceeding through two main strategies, i. e. chirality transfer from nonhelical enantioenriched precursors and stereoselective cycloaddition or annulation from achiral precursors, have enabled the enantioselective access to certain types of carbo- and heterohelicenes.[11] In recent years, C–H bond functionalisation has emerged as a powerful and step-economical approach to synthesise complex functional molecules, including polyaromatic systems of interest for organic materials.[18–20] Recently, a number of catalytic enantioselective C–H activation methods have been developed, proving particularly efficient and versatile for the control of diverse stereogenic elements including centres, planes and axes.[21,22] Despite intrinsic reactivity and

selectivity issues, such approaches would be particularly appealing for the synthesis of nonracemic helicenes. Recently, You and co-workers reported the enantioselective synthesis of azoniahelicenes via Rh-catalysed C–H annulation of fused isoquinolines with alkynes.[23] In addition, Ackermann and co-workers reported an indirect access to enantioenriched carbohelicenes involving an initial Pd-catalysed atroposelective C–H alkenylation, followed by conversion of the corresponding axially chiral biaryls to helicenes in three steps.[24] Despite all these advances, a one-step enantioselective entry into lower, nonfused carbo[*n*]helicenes from achiral precursors is still lacking. Palladium(0)-catalysed C–H arylation could potentially contribute to filling this gap (Fig. 1b).[25] Indeed, the control of axial chirally in (hetero)biaryls was recently reported by the groups of Cramer and Baudoin via such intramolecular[26] and intermolecular[27] reactions. Moreover, we showed that enantioselective Pd^0-catalysed C–H arylation allows the construction of warped polyaromatic systems.[28] Some of the obtained products adopted a helical shape reminiscent to helicenes, but which was in fact induced by the generated stereogenic centre. Key to the success of this method was the design of a bifunctional chiral ligand incorporating both a phosphine and a carboxylate moiety,[29] the former enabling a strong binding to the Pd center and the latter performing the C–H bond cleavage via concerted metalation-deprotonation.[30] This bifunctional catalyst features a highly organized chiral pocket, which seems to be well adapted to the enantioselective recognition of polyaromatic substrates via noncovalent interactions.[28,29] These features should therefore make this system also suitable to the enantioselective construction of helicenes. When considering this possibility, we were encouraged by precedents demonstrating the feasibility of helicene synthesis in the racemic mode,[31,32] despite a limited efficiency and generality. Such limitations can be expected from the high steric repulsion and strain energy at the critical C–H activation and C–C coupling steps of the catalytic cycle. Another foreseeable problem in the development of such an enantioselective C–H arylation method is the low racemisation energy barriers for lower

carbo[*4*]- ($\Delta G^{\ddagger}_{rac}$ 4.1 kcal mol^{-1}) and [*5*]helicenes ($\Delta G^{\ddagger}_{rac}$ 24.1 kcal mol^{-1}).[33] This problem can be circumvented through the design of suitable starting materials incorporating substituents on one of the peripheral rings, but potentially at the expense of reactivity.

Herein, we report the development of an efficient asymmetric C–H arylation method, which enables the synthesis of all lower carbo[*n*]helicenes (*n* = 4–6) from achiral precursors in a single step with generally excellent yields and enantioselectivities (e.r. up to 98:2, Fig. 1c). DFT calculations shed light on a complex mechanistic pathway in which both the C–H activation and reductive elimination steps have an impact on the enantioselectivity. Moreover, as this method enabled the access to scarcely reported configurationally stable carbo[*4*]helicenes, it led to an experimental comparative study of the photophysical and chiroptical properties of carbo[*4*], [*5*] and [*6*]helicenes, which revealed the high value of the dissymmetry factors of the smallest of these congeners.

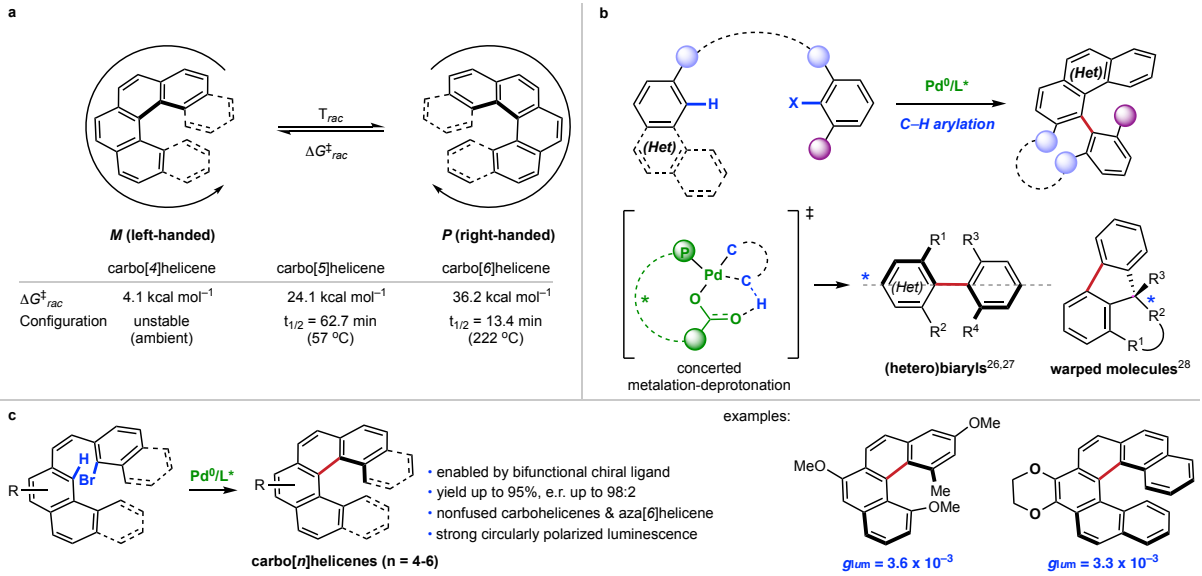

Fig. 1 Design of an enantioselective synthesis of carbo[*n*]helicenes by Pd^0-catalysed C–H arylation. a, Racemisation barriers for carbo[*4*], [*5*], and [*6*]helicenes. **b**, Pd^0-Catalysed enantioselective C–H arylation for the synthesis of axially chiral biaryl compounds, warped molecules, and the underlying CMD process. **c**, This work: synthesis of CPL-active lower carbo[*n*]helicenes by Pd^0-catalysed C–H arylation. e.r., enantiomeric ratio.

Results and discussion

Method development. Based on the known stability of unsubstituted carbo[*6*]helicene (Fig. 1a), 3,4-difluorohexahelicene (**2r**) was deemed to possess sufficient stability to withstand prolonged periods of heating at 140 °C without significant racemisation (Fig. 2). Hence, we started to study the C–H arylation of substrate **1r**, wherein the bromonaphthalene and phenanthrene rings are bridged by a (*Z*) olefin, and wherein fluorine atoms were installed on the phenanthrene ring to avoid undesired competitive C–H arylation on the latter, leading to the non-helicene product (*vide infra*). Bifunctional binaphthyl-based chiral phosphine-carboxylic acids quickly emerged as the most promising ligands,[28,29] as compared to monofunctional ligands – including binaphthyl-based ones – in combination with an external carboxylic acid co-catalyst (ESI, Fig. S1). Optimisation studies on the ligand structure revealed a significant yield improvement when a phenyl group was introduced at the 3-position of the binaphthyl core (in green). In addition, 3,5-disubstitution of the aryl substituents on phosphorus was found beneficial to the enantioselectivity (in blue). In particular, methyl substituents (**L^1**) provided a higher yield (84%) and an e.r. of 91:9, whereas *tert*-butyl substituents (**L^2**) provided a markedly enhanced e.r. of 98:2, albeit with a lower yield (45%). Substitution at the α-position to the carboxylic acid (in red) or partial saturation of the binaphthyl core (in purple) led to detrimental or marginal effects on yield and enantioselectivity. Further optimisations of the base and solvent led to the standard conditions indicated in Fig. 2, and both ligands **L^1**-**L^2** were kept for subsequent studies.

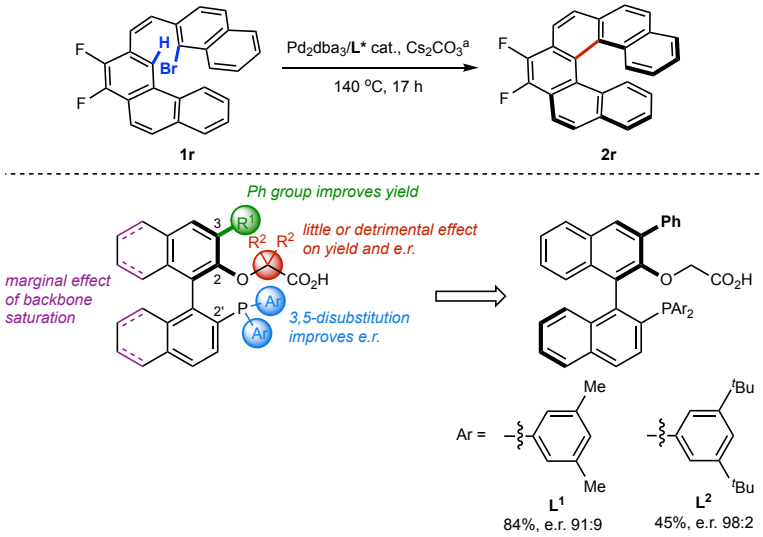

Fig. 2 Ligand structure-activity relationship in the enantioselective synthesis of carbo[*6*]helicene 2r. [a] Optimized conditions: **1r** (0.1 mmol, 1.0 equiv), Pd_2dba_3 (5 mol%), ligand (20 mol%), Cs_2CO_3 (0.5 equiv), CPME (1 mL), 17 h. E.r. were determined by HPLC on a chiral stationary phase. CPME, cyclopentyl methyl ether.

Scope of the enantioselective synthesis of carbo[*4*], [*5*] and [*6*]helicenes. Using the optimal conditions, we examined the versatility of the enantioselective C–H arylation for the synthesis of lower carbo[*n*]helicenes (Fig. 3). Due to the low racemisation barrier of unsubstituted carbo[*4*] and [*5*]helicenes, at least one of the terminal positions of the fjord region was blocked with a substituent to generate configurationally stable products. The racemisation barriers were calculated to be 35.6–40 kcal mol^{-1} for representative carbo[*n*]helicenes **2a**, **2h** and **2r** (Fig. S119-S121), consistent with literature values,[33] which indicated that the various products should indeed possess sufficient configurational stability under the reaction conditions. The precursors **1** were synthesized using a Wittig reaction to set up the required *Z* alkene linker between the two aryl fragments (see the ESI). In addition, as illustrated with **2g**, the current strategy requires to block the most reactive *ortho* position to the alkene on the naphthalene ring (C7 position on the helicene product) to avoid cyclisation on this less hindered position, which readily furnishes the corresponding benzanthracene system. These precautions pending, the scope of the reaction was explored using $\mathbf{L^1}$ as the preferred ligand. For some cases, $\mathbf{L^2}$ was employed to reach higher enantioselectivities.

First, a range of carbo[*4*]helicenes were successfully synthesized through intramolecular C–H arylation of substituted naphthalenes with *ortho*-substituted phenyl bromide precursors, which occurred at 120 °C using $\mathbf{L^1}$ as the chiral ligand. Different terminal groups, including methyl, methoxy and isopropoxy groups were found suitable (**2a-b**). Substrates containing electron-donating or -withdrawing groups on the bromobenzene ring readily participated in this reaction to afford products **2c-f**. Remarkably, all carbo[*4*]helicene products were obtained in similarly excellent yields (90-95%) and enantioselectivities (e.r. 93:7-96:4).

The reaction was also applicable to carbo[*5*]helicenes, wherein only one blocking substituent on a terminal ring of the fjord region is in principle necessary to obtain configurationally stable products. To this purpose, the intramolecular C–H arylation of phenanthrenes with *ortho*-substituted phenyl bromides was first considered in analogy to carbo[*4*]helicenes. A methyl (**2h**) or isopropoxy (**2i**) group at the *ortho* position to the initial bromide provided excellent results. However, a methoxy substituent at this position of the fjord region led to a product (**2q**) which slowly racemized at 120 °C. The racemisation barrier ($\Delta G^{\ddagger}_{rac}$) of **2q** was measured to be 34.6 kcal mol^{-1} in toluene (see the ESI), hence confirming the lower configurational stability of this particular product (as compared with **2h**). In this case, decreasing the reaction time to 9 h was sufficient to limit this racemisation, and **2q** was obtained in 93:7 e.r. The absolute configuration of **2q** was determined by X-ray crystallographic analysis to be (*M*). Diverse substituents at the terminal (**2j-n**) and central (**2h**, **2o-p**) rings of the incipient carbo[*5*]helicene were very well tolerated, affording again excellent yields (81-92%) and e.r. values up to 97:3. In some instances, a very high optical purity (e.r. >99.5:0.5) was easily reached by simple recrystallisation of the product (**2o**, **2p** and **2q**). Of note, product **2q** was obtained from a naphthalene-bromonaphthalene precursor instead of a phenanthrene-bromobenzene. This type of substrates allows access to a carbo[*5*]helicene with an unsubstituted central ring, which

highlights the flexibility of the current method to access carbohelicenes with different substitution patterns.

Compared to carbo[*4*] and [*5*]helicenes, carbo[*6*]helicenes have larger extended π-surfaces, which makes the reaction more challenging. In this case, we investigated the C–H arylation of substituted phenanthrenes with *ortho*-substituted naphthyl bromides, and both $\mathbf{L^1}$ and $\mathbf{L^2}$ were tested to achieve optimal results. Ligand $\mathbf{L^1}$ consistently produced high yields (68-93%) and around 90:10 e.r. (**2r-x**), whereas with $\mathbf{L^2}$ the yields were lower but the enantioselectivity was markedly improved (**2r**, **2u-w**, e.r. 94:6-98:2). Similar to carbo[*5*]helicenes, the optical purity could be further improved upon recrystallisation (**2u**). Azahelicenes are important heteroanalogues of carbohelicenes with interesting chiroptical properties.[7,34] In light of this interest, a bromoquinoline (**1x**) was also prepared and tested to further probe the versatility of the developed catalytic enantioselective protocol beyond carbohelicenes. Gratifyingly, the corresponding aza[*6*]helicene (**2x**) was obtained in 75% yield and 90:10 e.r., and could be further enantioenriched upon recrystallisation.

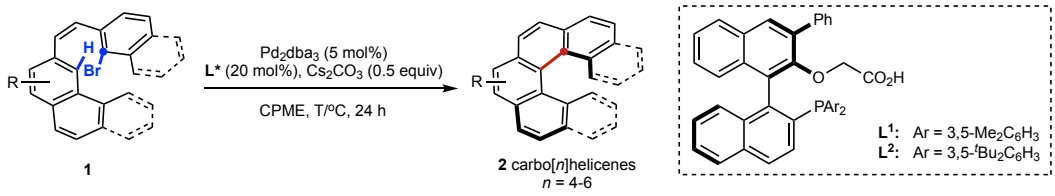

[4]helicenes: L¹, 120 °C

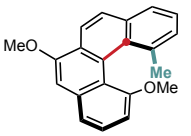

2a
93%, e.r. 93:7
$\Delta G^{\ddagger}rac$ = 35.6 kcal mol^{-1} [a]

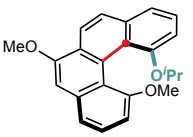

2b
92%, e.r. 96:4

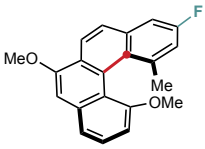

2c
94%, e.r. 94:6

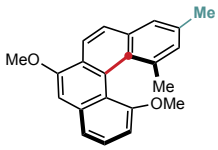

2d
95%, e.r. 95:5

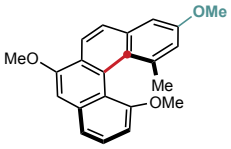

2e
90%, e.r. 95:5

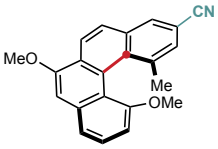

2f
95%, e.r. 95:5

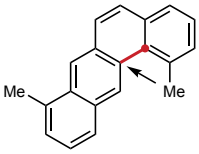

2g
85%

[5]helicenes

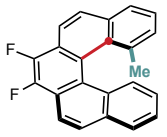

2h
L¹, 140 °C
85%, e.r. 95:5
$\Delta G^{\ddagger}rac$ = 40.0 kcal mol^{-1} [a]

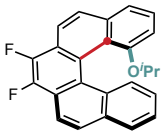

2i
L², 140 °C, 13.5 h
91%, e.r. 97:3

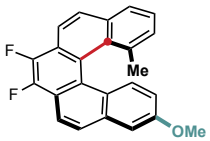

2j
L¹, 140 °C
92%, e.r. 94:6

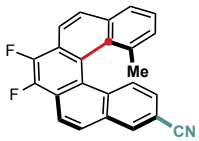

2k
L¹, 140 °C
88%, e.r. 95:5

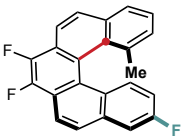

2l
L¹, 140 °C
92%, e.r. 95:5

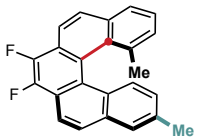

2m
L¹, 140 °C
91%, e.r. 94:6

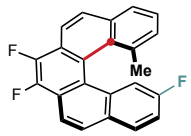

2n
L¹, 140 °C
81%, e.r. 92:8

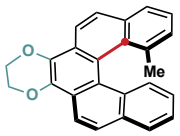

2o
L¹, 140 °C
94%, e.r. 91:9
>99.5:0.5 after recryst.

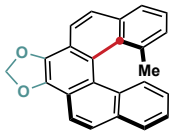

2p
L¹, 140 °C
95%, e.r. n.d.
e.r. >99.5:0.5 after recryst.

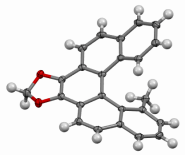

X-ray structure[c]
2p

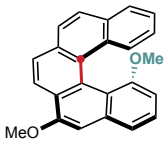

2q
L¹, 120 °C, 9 h
91%, e.r. 93:7
e.r. >99.5:0.5 after recryst.
$\Delta G^{\ddagger}rac$ = 34.6 kcal mol^{-1} [b]

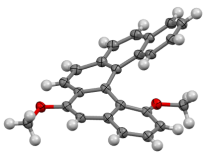

X-ray structure[d]
2q

[6]helicenes

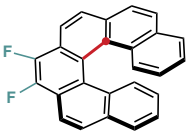

2r
L¹, 140 °C
84%, e.r. 91:9
L², 140 °C
45%, e.r. 98:2
$\Delta G^{\ddagger}rac$ = 38.1 kcal mol^{-1} [a]

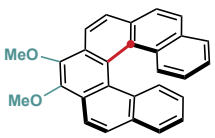

2s
L¹, 140 °C
70%, e.r. 92:8

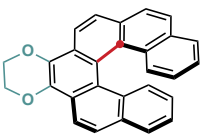

2t
L¹, 140 °C
73%, e.r. 90:10

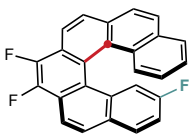

2u
L¹, 140 °C
68%, e.r. 88:12
e.r. >99.5:0.5 after recryst.
L², 140 °C
42%, e.r. 97:3

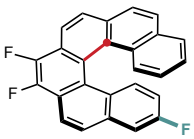

2v
L¹, 140 °C
91%, e.r. 93:7
L², 140 °C
39%, e.r. 94:6

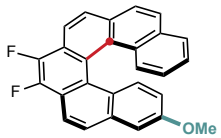

2w
L¹, 140 °C
93%, e.r. 93:7
L², 140 °C
40%, e.r. 94:6

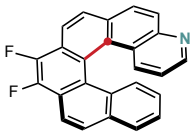

2x
L¹, 140 °C
75%, e.r. 90:10
e.r. >99.5:0.5 after recryst.

Fig. 3 Scope of the enantioselective synthesis of carbo[*4*], [*5*] and [*6*]helicenes. Standard conditions: **1a** (0.1 mmol, 1.0 equiv), Pd_2dba_3 (5 mol%), ligand (20 mol%), Cs_2CO_3 (0.5 equiv), CPME (1 mL). E.r. were determined by HPLC on a chiral stationary phase. The reference racemic products were synthesized using PCy_3 instead of the chiral ligand. The absolute configurations were ascribed in analogy to **2p** and **2q** and by comparing the calculated

with the experimental ECD spectra for selected compounds. The red dots indicate the initial position of the bromide. [a] Free energy of racemisation computed at the B3LYP-D3(BJ)/6-311G(d,p) level of theory. [b] Experimental racemisation barrier. [c] Thermal ellipsoids shown at 50% probability. [c] Thermal ellipsoids shown at 20% probability.

Mechanistic study.

Density functional theory (DFT) calculations were performed to understand how the chiral bifunctional ligands induce enantioselectivity in the reaction. Because of the initial data obtained with substrate **1r**, the corresponding oxidative addition complexes **I-L^n** (n = 1, 2) were chosen as models in these mechanistic studies (Fig. 4). Depending on how the substrate is positioned in the metal complexes, two isomers are observed, **I-L^n** and **I*-L^n**. Complex **I-L^1** undergoes C−H activation via **I-TS-L^1** with $\Delta G^{\ddagger}$ = 25.7 kcal mol^{-1} to form **II-L^1** (bottom), whereas C−H activation from **I*-L^1** via **I*-TS-L^1** requires a higher activation energy by $\Delta\Delta G^{\ddagger}$ = 1.2 kcal mol^{-1} than **I-TS-L^1** to form **II*-L^1** (top). This concerted metalation-deprotonation was computed to feature the highest activation barrier of the energy profile (see Fig. S2-S3 for the overall reaction profiles with **L^1-L^2**). On the other hand, the barrier for the C−H activation from **I-L^2** is $\Delta G^{\ddagger}$ = 26.3 kcal mol^{-1} via **I-TS-L^2**, whereas **I*-L^2** requires a lower barrier by only $\Delta\Delta G^{\ddagger}$ = –0.4 kcal mol^{-1} via **I*-TS-L^2** (see the ESI for a detailed analysis). The low $\Delta\Delta G^{\ddagger}$ energy differences between these two C–H activation pathways imply that they both play a role in the stereochemical outcome of the reaction. Then, deprotonation of the complexes **II-L^n** and **II*-L^n** with cesium bicarbonate and Cs^+ coordination is exergonic and provides complexes **III-L^n** and **III*-L^n**, respectively.

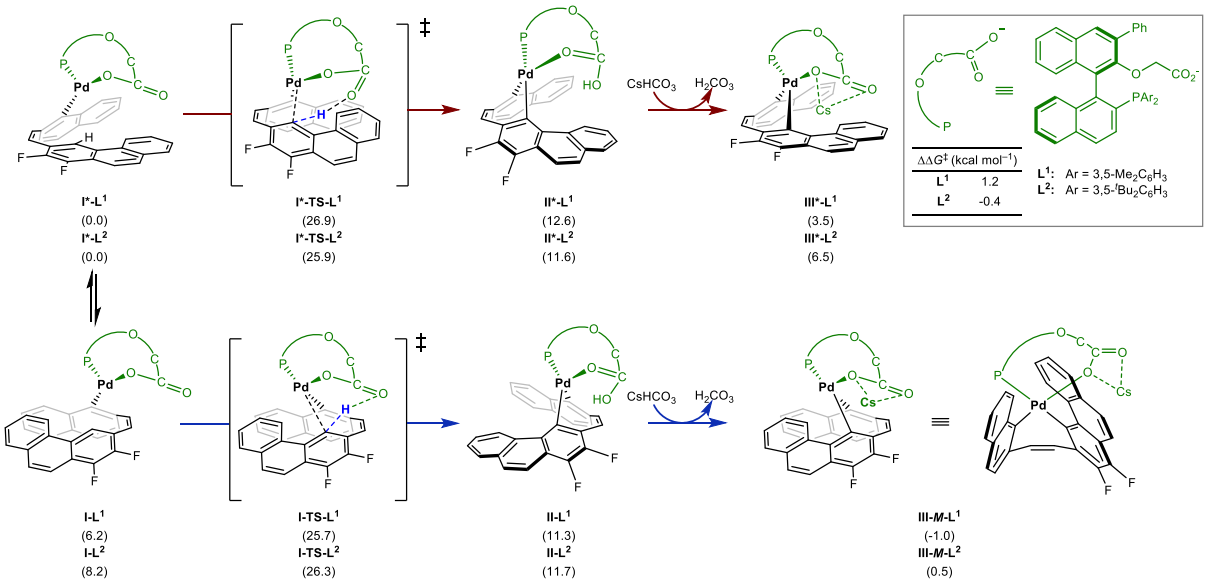

Fig. 4 Computed C–H activation pathways at PCM(toluene)-B3LYP(D3)/SDD+6-311+G**//B3LYP(D3)/LANL2DZ+6-31G** level of theory (ΔG in kcal mol^{-1}). TS, transition state. Cartesian coordinates for the optimized structures are provided in the ESI.

Next, the reductive elimination from the first complex **III-L^n** was computed to proceed via **III-TS$_M$-L^n** or **III-TS$_P$-L^n**, hence producing the (*M*) and (*P*) carbo[*6*]helicene **2r**, respectively (Fig. 5a). The corresponding activation barriers were calculated to be $\Delta G^{\ddagger}$ = 12.0 kcal mol^{-1} for **III-TS$_M$-L^1** and $\Delta G^{\ddagger}$ = 16.5 kcal mol^{-1} for **III-TS$_P$-L^1**, hence strongly favoring the experimentally observed major (*M*) enantiomer of **2r**. To reveal the origins of the enantioselectivity, the optimized TS structures of the reductive elimination were carefully analysed. We observed that noncovalent interactions between the catalyst and substrate strongly influence the enantiodetermining process (Fig. 5a).[35–38] As shown with NCI plots (Fig. S6),[39] both **III-TS$_M$-L^1** and **III-TS$_P$-L^1** display cation/π interactions between Cs^+ and the phenanthrene,[40] with a distance of 3.70(3) Å and 3.69(8) Å, respectively. The difference in relative strengths of these Cs^+/π interactions is marginal between these TSs based on the distances. However, a notable C–H/π interaction between the phenanthrene ring of the substrate and one of the *m*-xylyl rings of the ligand is found to be operative in **III-TS$_M$-L^1**, while **III-TS$_P$-L^1** does not feature such an interaction. This interaction might explain the experimentally observed effect of this aryl substituent of the ligand on the enantioselectivity (see Fig. 2). In addition, the cesium

carboxylate moiety in **III-TS$_M$-L^1**, with the substrate phenanthrene ring being tilted upward, is positioned in a more staggered arrangement with a dihedral angle O^1–C^1–C^2–O^2 of 22.6°, wherein the optimal Cs^+/π interaction is attained. In contrast, **III-TS$_P$-L^1** involves a dihedral angle $O^{1'}$–$C^{1'}$–$C^{2'}$–$O^{2'}$ of 11.4° to maintain the analogous Cs^+/π interaction. In consequence, the staggered conformation in **III-TS$_M$-L^1** places O^1 relatively closer to Pd to give a shortened Pd···O^1 distance of 2.38 Å, contributing to the stabilisation of the TS, as compared with **III-TS$_P$-L^1** which features a longer Pd···$O^{1'}$ distance of 2.49 Å. Another stark difference was identified in the forming $C^{3(')}$–$C^{4(')}$ bonds in **III-TS$_M$-L^1** and **III-TS$_P$-L^1**, with a distance of 1.96 Å and 2.15 Å, respectively. This difference indicates that **III-TS$_M$-L^1** is a later TS and takes advantage of aromatisation, which contributes to the facile formation of the (*M*) carbohelicene. Similarly, we could locate two diastereoisomeric TSs from intermediate **III*-L^1** obtained through the second C–H activation pathway, **III*-TS$_M$-L^1** and **III*-TS$_P$-L^1**, with the former being kinetically more accessible by 4.5 kcal mol^{-1} than the latter, hence also favouring the (*M*) carbohelicene product (Fig. 5b). This energy difference between these two TSs can be related to the different torsion angles $C^{5(')}$–$C^{6(')}$–$C^{7(')}$–$C^{8(')}$ of the phenyl-naphthyl moiety of the ligand.[41,42] Whereas **III*-TS$_M$-L^1** involves a favourable torsion angle C^5–C^6–C^7–C^8 of 48.9°, the phenyl-naphthyl system in **III*-TS$_P$-L^1** displays a lower torsion angle $C^{5'}$–$C^{6'}$–$C^{7'}$–$C^{8'}$ of 38.2° in order to avoid the steric collision with the phenanthrene ring of the substrate. In addition, **III*-TS$_P$-L^1** exhibits a deviation from the ideal square-planar geometry, which must occur to avoid the steric clash between the ligand and the phenanthrene ring of the substrate. In contrast, **III*-TS$_M$-L^1** lacks such a steric repulsion, with the phenanthrene ring being positioned away from the phenyl-naphthyl moiety of the ligand. The reductive elimination TSs from intermediates **III-L^2** and **III*-L^2**, which are qualitatively similar to those observed with **L^1**, are fully illustrated in Fig. S7.

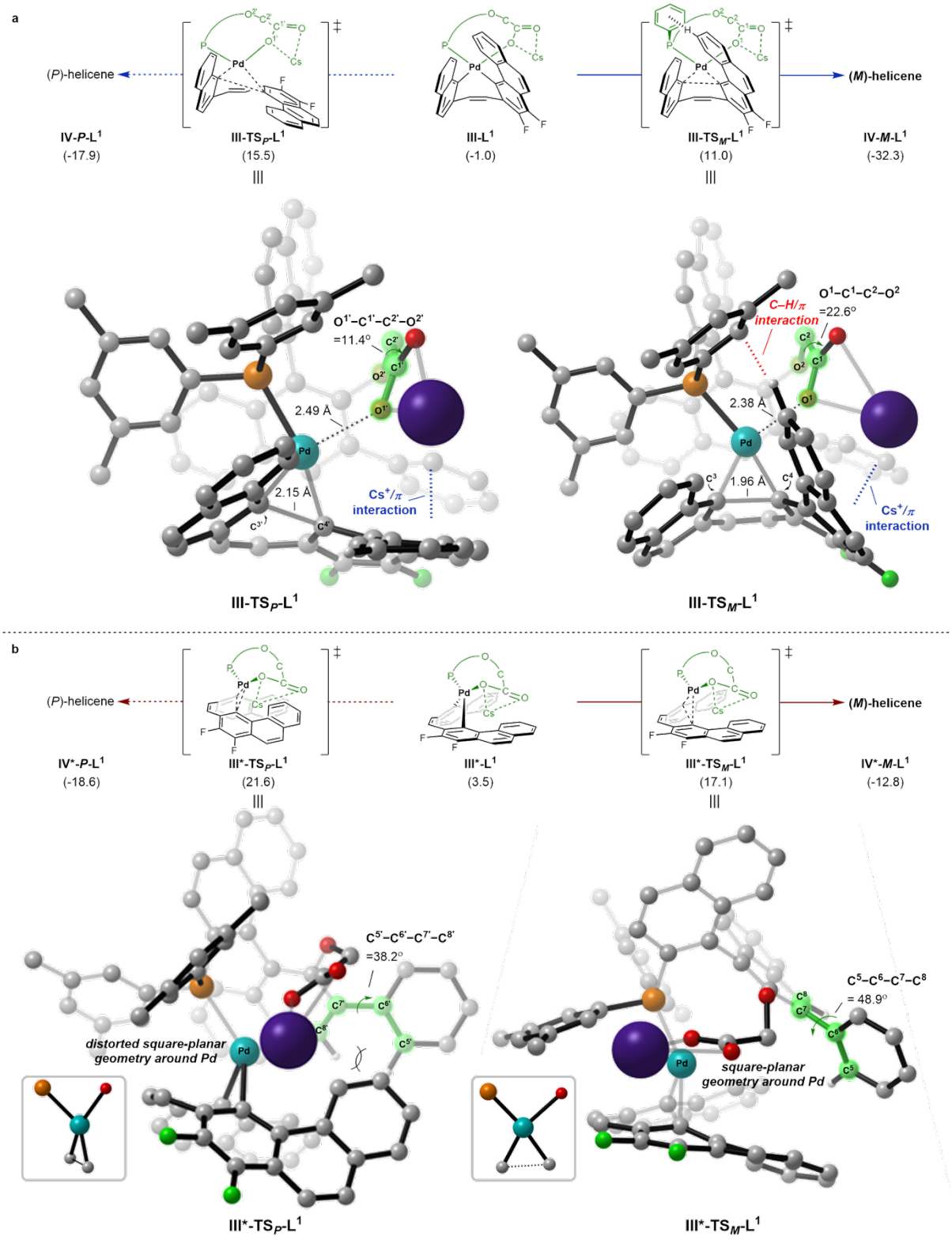

Fig. 5 Computed reductive elimination pathways leading to carbo[*6*]helicene **2r** with $\mathbf{L^1}$ as the ligand at PCM(toluene)-B3LYP(D3)/SDD+6-311+G**//B3LYP(D3)/LANL2DZ+6-31G** level of theory. Bold lines represent the favored pathway. For reductive elimination pathways with $\mathbf{L^2}$ and selected NCI plots, see Fig. S6-S7. **a,** reductive elimination from **III-L^1**. **b,** reductive elimination from **III*-L^1**.

Since the diastereoisomeric TSs in each pathway display lower barriers than those of the C–H activation step, the current calculations indicate that the reductive elimination step is enantiodetermining. However, since the two C–H activation TSs have a comparable energy for both ligands $\mathbf{L^1}$ and $\mathbf{L^2}$, this step also has an impact on the quantitative product distribution, hence reflecting the complexity of the reaction dynamics. Moreover, both C–H activation pathways are computed to strongly favor the (*M*) enantiomer, whereas a lower energy difference in favor of the (*M*) enantiomer is observed experimentally. We believe that this discrepancy reflects the molecular and dynamic complexity of the current system, which is difficult to compute with a great accuracy.

Study of photophysical and chiroptical properties.

A study of the photophysical and chiroptical properties of selected carbohelicenes was performed in dichloromethane by means of ultraviolet–visible, fluorescence (including prompt photoluminescence quantum yield (PLQY) and fluorescence lifetime measurements), electronic circular dichroism (ECD) and CPL spectroscopies. In addition, TD-DFT calculations were performed on selected compounds (**2a**, **2c**, **2p**, **2u**), validating the (*M*) absolute configurations reported in Fig. 3, using the ECD fingerprints (Fig. S122-S125). The dissymmetry factors at the excited state (g_{lum}) are reported in Fig. 6 and the PLQY in Fig. S118.

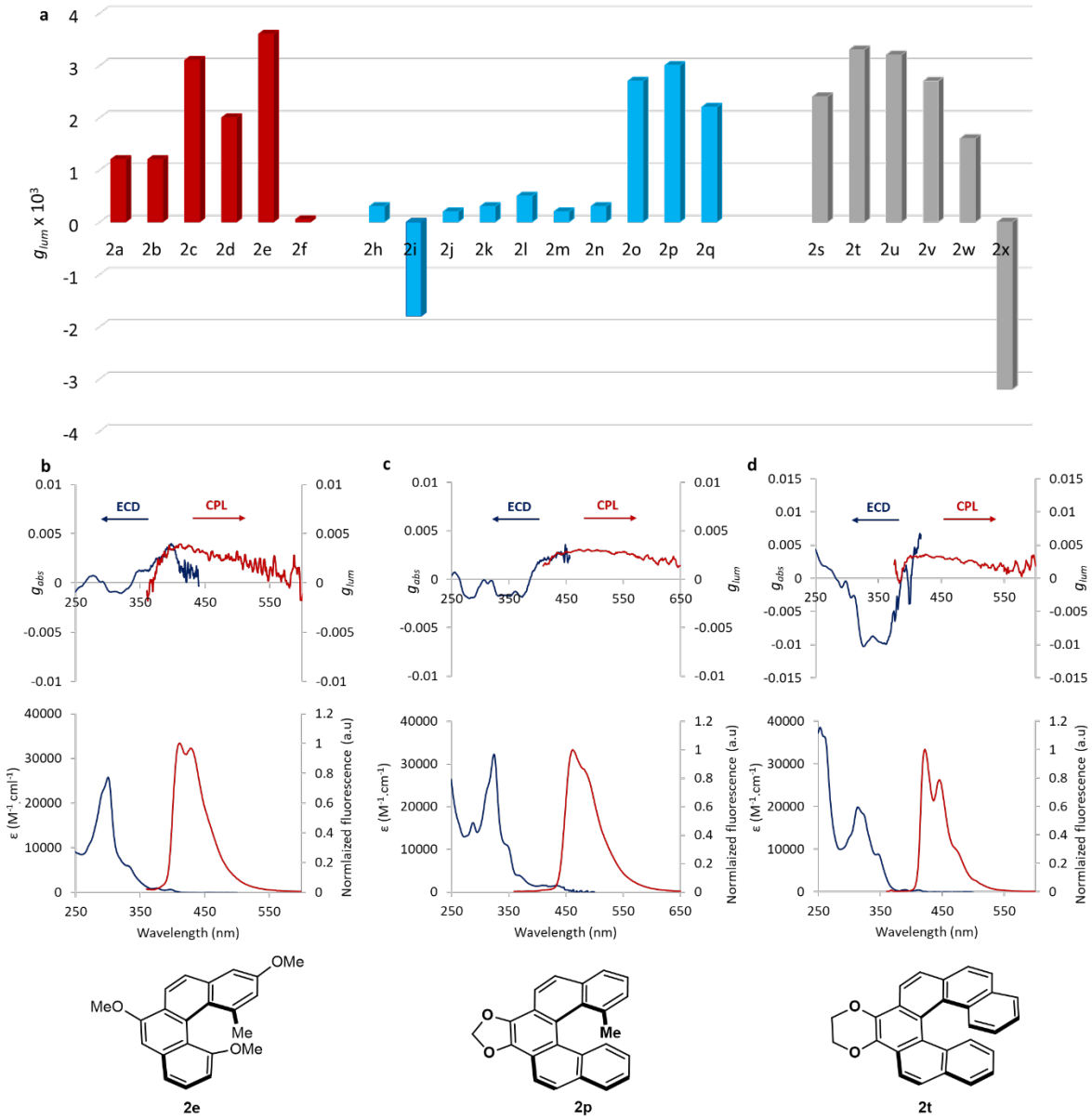

Fig. 6. **a,** Dissymmetry factors (at λ_{max}(em)) of selected synthesized helicenes in dichloromethane (c = 10^{-5} M). Red bars, [*4*]helicenes, blue bars, [*5*]helicenes, grey bars, [*6*]helicenes. **b, c, d,** top: g_{abs} = f (λ), blue traces, and g_{lum} = f (λ) curves, red traces; bottom: UV-vis, blue traces, and luminescence spectra, red traces, of selected carbohelicenes **2c**, **2p** and **2t**, respectively.

For all compounds, the nature and position of the substituents only slightly affected the emission maxima λ_{max}(em), which ranged from 420-440 nm and mostly depended on the helicene length. The measured PLQYs (with an integrating sphere) are in line with those reported for carbohelicenes,[43] with values in the range of 2-13 %. Of note, the presence of a fused dioxolane or dioxane ring on both carbo[*5*]- and [*6*]helicenes (**2o**, **2p**, **2t**) provided among the highest PLQY values (9.3-10 %). Some substitution patterns also positively affected the

g_{lum} values. Indeed, in the carbo[*4*]helicene series, adding a substituent in the 3-position led to a significant increase of the g_{lum} (**2a**, 1.0 × 10^{-3}; **2d**, 1.8 × 10^{-3}; **2c**, 3.1 × 10^{-3}; **2e**, 3.6 × 10^{-3}). While the presence of the nitrile group positively influenced the PLQY of **2f** (13% vs 8% for **2a**), it was deleterious to the g_{lum} value, reaching only 0.1-0.2 × 10^{-3} at the emission maximum (bisignated CPL signal, Fig. S35). The carbo[*5*]helicenes displayed the lowest g_{lum} values in average (0.2-0.5 × 10^{-3}), except for **2o**, **2p** and **2q** (2.2-3.0 × 10^{-3}), suggesting a detrimental effect of a fluorine atom in positions 7 and 8 on the chiroptical properties. Surprisingly, the substitution pattern in **2i** led to a sign inversion of the emitted CPL compared to the other carbohelicenes. In the carbo[*6*]helicene series, g_{lum} values were found to be less affected by the substitution pattern. Interestingly, the aza[*6*]helicene **2x** displayed a sign inversion of the CPL compared to the studied carbo[*6*]helicenes, as well as an enhancement of the dissymmetry factor (reaching –5.4 × 10^{-3} at the beginning of the emission signal, Fig. S51). The most important conclusion of this comparative experimental study is probably the unexpectedly high g_{lum} values measured for the carbo[*4*]helicenes, above 3 × 10^{-3} for compounds **2c** and **2e**, which are comparable to their [*6*]helicene congeners. This result highlights the potential of these configurationally stable lower helicenes for the development of small molecules displaying strong chiroptical responses.

Conclusion

A general enantioselective access to lower carbo[*n*]helicenes was developed using Pd^0-catalysed C–H arylation in the presence of a chiral phosphine-carboxylate bifunctional ligand. This method provides good yields and high enantioselectivities (e.r. up to 98:2) across a broad range of helicene products, and was also found applicable to an aza[*6*]helicene. Computational studies shed light on the reaction mechanism, in particular on the contribution of both the C–H activation and reductive elimination steps to the overall enantioselectivity. In addition, a combination of noncovalent interactions and steric repulsion between the substrate and ligand

was shown to be responsible for the enantio-induction during the two key reductive elimination steps. A comparative study of the photophysical and chiroptical properties of selected helicene products showed a surprisingly high CPL response for the lowest carbo[*4*]helicene congeners, comparable to carbo[*6*]helicenes and higher than carbo[*5*]helicenes. Since the synthetic access to the former is relatively straightforward, these results suggest new avenues for the optimisation of chiroptical properties of helicene systems.

Data availability. Data supporting the findings of this study are available in the Supplementary Information or from the corresponding author upon request. The Supplementary Information contains full details on the synthesis, characterisation of compounds and computational studies. CCDC 2142962 (compound **2p**) and 2142961 (compound **2q**) contains the supplementary crystallo- graphic data for this paper. These data can be obtained free of charge from The Cambridge Crystallographic Data Centre via https://www.ccdc.cam.ac.uk/structures/.

References

1. Chen, C. F. & Shen, Y. Helicene chemistry: from synthesis to applications. Springer-Verlag: Berlin (2017).
2. Gingras, M. One hundred years of helicene chemistry. Part 3: applications and properties of carbohelicenes. *Chem. Soc. Rev.* **42**, 1051–1095 (2013).
3. Aillard, P., Voituriez, A. & Marinetti, A. Helicene-like chiral auxiliaries in asymmetric catalysis. *Dalton Trans*. **43**, 15263–15278 (2014).
4. Ravat, P., Šolomek, T. & Juríček, M. Helicenes as chiroptical photoswitches. *ChemPhotoChem.* **3**, 180–186 (2019).
5. Ernst, K.-H. Stereochemical recognition of helicenes on metal surfaces. *Acc. Chem. Res*. **49**, 1182−1190 (2016).

6. Zhao, H., Xu, X., Zhou, L., Hu, Y., Huang, Y. & Narita, A. Water-soluble nanoparticles with twisted double [7]carbohelicene for lysosome-targeted cancer photodynamic therapy. *Small* **18**, 2105365 (2022).
7. Dhbaibi, K., Favereau, L. & Crassous, J. Enantioenriched helicenes and helicenoids containing main-group elements (B, Si, N, P). *Chem. Rev.* **119**, 8846−8953 (2019).
8. Zhao, W.-L., Li, M., Lu, H.-Y. & Chen, C.-F. Advances in helicene derivatives with circularly polarized luminescence. *Chem. Commun.* **55**, 13793–13803 (2019).
9. Gingras, M. One hundred years of helicene chemistry. Part 1: non-stereoselective syntheses of carbohelicenes. *Chem. Soc. Rev.* **42**, 968−1006 (2013).
10. Shen, Y. & Chen, C.-F. Helicenes: synthesis and applications. *Chem. Rev.* **112**, 1463–1535 (2012).
11. Gingras, M. Félix, G. & Peresutti, R. One hundred years of helicene chemistry. Part 2: stereoselective syntheses and chiral separations of carbohelicenes. *Chem. Soc. Rev.* **42**, 1007−1050 (2013).
12. Kötzner, L., Webber, M. J., Martínez, A., De Fusco, C. & List, B. Asymmetric catalysis on the nanoscale: the organocatalytic approach to helicenes. *Angew. Chem. Int. Ed.* **53**, 5202–5205 (2014).
13. Liu, P., Bao, X., Naubron, J.-V., Chentouf, S., Humbel, S., Vanthuyne, N., Jean, M., Giordano, L., Rodriguez, J. & Bonne, D. Simultaneous control of central and helical chiralities: expedient helicoselective synthesis of dioxa[6]helicenes. *J. Am. Chem. Soc.* **142**, 16199−16204 (2020).
14. Nakamura, K., Furumi, S., Takeuchi, M., Shibuya, T. & Tanaka, K. Enantioselective synthesis and enhanced circularly polarized luminescence of S-shaped double azahelicenes. *J. Am. Chem. Soc*. **136**, 5555−5558 (2014).

15. Hartung, T., Machleid, R., Simon, M., Golz, C. & Alcarazo, M. Enantioselective synthesis of 1,12-disubstituted [4]helicenes. *Angew. Chem. Int. Ed.* **59**, 5660–5664 (2020).

16. Šámal, M., Chercheja, S., Rybáček, J., Vacek Chocholoušová, J., Vacek, J., Bednárová, L., Šaman, D., Stará, I. G. & Starý, I. An ultimate stereocontrol in asymmetric synthesis of optically pure fully aromatic helicenes. *J. Am. Chem. Soc.* **137**, 8469–8474 (2015).

17. Yubuta, A., Hosokawa, T., Gon, M., Tanaka, K. Chujo, Y., Tsurusaki, A. & Kamikawa, K. Enantioselective synthesis of triple helicenes by cross-cyclotrimerisation of a helicenyl aryne and alkynes via dynamic kinetic resolution. *J. Am. Chem. Soc*. **142**, 10025−10033 (2020).

18. Segawa, Y., Maekawa, T. & Itami, K. Synthesis of extended π-systems through C–H activation. *Angew. Chem. Int. Ed.* **54**, 66–81 (2015).

19. Ito, H., Ozaki, K. & Itami, K. Annulative π-extension (APEX): rapid access to fused arenes, heteroarenes, and nanographenes. *Angew. Chem. Int. Ed.* **56**, 11144–11164 (2017).

20. Li, B., Ali, A. I. M. & Ge, H. Recent advances in using transition-metal-catalysed C–H functionalisation to build fluorescent materials. *Chem* **6**, 2591–2657 (2020).

21. Newton, C. G., Wang, S.-G. Oliveira, C. C. & Cramer, N. Catalytic enantioselective transformations involving C−H bond cleavage by transition-metal complexes. *Chem. Rev*. **117**, 8908−8976 (2017).

22. Saint-Denis, T. G., Zhu, R.-Y., Chen, G., Wu, Q.-F. & Yu, J.-Q. Enantioselective C(sp^3)–H bond activation by chiral transition metal catalysis. *Science* **359**, eaao4798 (2018).

23. Wang, Q., Zhang, W.-W., Zheng, C., Gu, Q. & You, S.-L. Enantioselective synthesis of azoniahelicenes by Rh-catalysed C−H annulation with alkynes. *J. Am. Chem. Soc.* **143**, 114−120 (2021).

24. Dhawa, U., Tian, C., Wdowik, T., Oliveira, J. C. A., Hao, J. & Ackermann, L. Enantioselective pallada-electrocatalysed C－H activation by transient directing groups: expedient access to helicenes. *Angew. Chem. Int. Ed*. **59**, 13451–13457 (2020).

25. Vyhivskyi, O., Kudashev, A., Miyakoshi, T. & Baudoin, O. Chiral catalysts for Pd^0-catalysed enantioselective C–H activation, *Chem. Eur. J.* **27**, 1231–1257 (2021).

26. Newton, C. G., Braconi, E., Kuziola, J., Wodrich, M. D. & Cramer, N. Axially chiral dibenzazepinones by a palladium(0)-catalysed atropo-enantioselective C−H arylation. *Angew. Chem. Int. Ed.* **57**, 11040−11044 (2018).

27. Nguyen, Q.-H., Guo, S.-M., Royal, T., Baudoin, O. & Cramer, N. Intermolecular palladium(0)-catalysed atropo-enantioselective C−H arylation of heteroarenes. *J. Am. Chem. Soc.* **142**, 2161−2167 (2020).

28. Savary, D. & Baudoin, O. Enantioselective Pd^0-catalysed C(sp^2)–H arylation for the synthesis of chiral warped molecules. *Angew. Chem. Int. Ed*. **60**, 5136–5140 (2021).

29. Yang, L., Neuburger, M. & Baudoin, O. Chiral bifunctional phosphine-carboxylate ligands for palladium(0)-catalysed enantioselective C−H arylation. *Angew. Chem. Int. Ed.* **57**, 1394–1398 (2018).

30. Ackermann, L. Carboxylate-assisted transition-metal-catalysed C–H bond functionalisations: mechanism and scope. *Chem. Rev.* **111**, 1315–1345 (2011).

31. Kamikawa, K., Takemoto, I., Takemoto, S. & Matsuzaka, H. Synthesis of helicenes utilizing palladium-catalysed double C–H arylation reaction. *J. Org. Chem*. **72**, 7406-7408 (2007).

32. Kelgtermans, H., Dobrza, L., Van Meervelt, L. & Dehaen, W. A fragment-based approach toward substituted trioxa[*7*]helicenes. *Org. Lett.* **14**, 5200–5203 (2012).

33. Ravat, P. Carbo[n]helicenes restricted to enantiomerize: an insight into the design process of configurationally stable functional chiral PAHs. *Chem. Eur. J*. **27**, 3957 –3967 (2021).

34. Yang, Y., Correa da Costa, R., Fuchter, M. J. & Campbell, A. J. Circularly polarized light detection by a chiral organic semiconductor transistor. *Nat. Photonics* **7**, 634–638 (2013).

35. Wagner, J. P. & Schreiner, P. R. London dispersion in molecular chemistry−reconsidering steric effects *Angew. Chem. Int. Ed.* **54**, 12274–12296 (2015).

36. Neel, A. J., Hilton, M. J., Sigman, M. S. & Toste, F. D. Exploiting non-covalent pi interactions for catalyst design. *Nature* **543**, 637–646 (2017).

37. Reddi, Y., Tsai, C.-C., Avila, C. M., Toste, F. D. & Sunoj, R. B. Harnessing noncovalent interactions in dual-catalytic enantioselective Heck–Matsuda arylation. *J. Am. Chem. Soc.* **141**, 998–1009 (2019).

38. Cornaton, Y. & Djukic, J.-P. Noncovalent interactions in organometallic chemistry: from cohesion to reactivity, a new chapter. *Acc. Chem. Res.* **54**, 3828–3840 (2021).

39. Johnson, E. R., Keinan, S., Mori-Sáchenz, P., Contreras-García, J., Cohen, A. J. & Yang, W. Revealing Noncovalent interactions. *J. Am. Chem. Soc.* **132**, 6498–6506 (2010).

40. Mahadevi, A. S. & Sastry, G. N. Cation−π interaction: its role and relevance in chemistry, biology, and material science. *Chem. Rev.* **113**, 2100–2138 (2013).

41. Johansson, M. P. & Olsen, J. Torsional barriers and equilibrium angle of biphenyl: reconciling theory with experiment. *J. Chem. Theory Comput.* **4**, 1460–1471 (2008).

42. Grein, F. Twist angles and rotational energy barriers of biphenyl and substituted biphenyls *J. Phys. Chem. A*, **106**, 3823–3827 (2002).

43. Birks, J. B., Birch, D. J. S., Cordemans, E., Vander Donckt, E. Fluorescence of the higher helicenes. *Chem. Phys. Lett.* **43**, 33–36 (1976).

Acknowledgements

This work was financially supported by the University of Basel. S.-M. Guo thanks the China Scholarship Council and S. Huh the State Secretariat for Education, Research and Innovation (2021.0174) for scholarships. We thank Dr. A. Prescimone, University of Basel, and Dr. F. Fadaei Tirani, Ecole Polytechnique Fédérale de Lausanne, for X-ray diffraction analyses, Dr. M. Devereux, University of Basel, for assistance with computing, Dr. D. Häussinger, University of Basel, for NMR experiments, S. Mittelheisser and Dr. M. Pfeffer, University of Basel, for MS analysis, Dr. Michel Massela, SCBM, for his help with computational resources.

Author contributions

S.-M.G. developed the catalytic method and performed the experiments, analysed experimental data, co-wrote the manuscript and ESI. S.H. conducted the mechanistic computational studies and co-wrote the manuscript and ESI. L.S. contributed to the synthesis of ligands and substrates. M.C. investigated the photophysical and chiroptical properties, G.P. performed TD-DFT and racemisation barrier calculations. M.C. and G.P. analysed the results and co-wrote the manuscript. O.B. directed the investigations and co-wrote the manuscript.

Competing interests

The authors declare no competing interests.